Liu, W., You, R., Zhang, J., and Chen, Q. 2017. "Development of a fast fluid dynamics-based adjoint method for the inverse design of indoor environments," *Journal of Building Performance Simulation*, 10(3): 326-343.

Development of a fast fluid dynamics-based adjoint method for the inverse design of indoor environments

Wei Liu[1,2], Ruoyu You[1], Jie Zhang[2], Qingyan Chen[1*]

[1]School of Mechanical Engineering, Purdue University, West Lafayette, IN 47907, USA
[2]Tianjin Key Laboratory of Indoor Air Environmental Quality Control, School of Environmental Science and Engineering, Tianjin University, Tianjin 300072, China

[*]Corresponding author:

Email: yanchen@purdue.edu
Address: School of Mechanical Engineering, Purdue University, 585 Purdue Mall, West Lafayette, IN 47907-2088
Phone: (765) 496-7562, FAX: (765) 494-0539

Abstract

The CFD-based adjoint method may be appropriate for the inverse design of indoor environments, considering both accuracy and efficiency, but a single design of an indoor space still requires tens of hours with the use of a personal computer. To speed up the inverse design process, this study evaluated four FFD models in terms of solving the Navier-Stokes equations, integration with turbulence models, and solving the adjoint equations. This study developed the FFD solvers in OpenFOAM and validated them for predicting steady-state and transient flow in indoor environments. The effect of the time step size was also investigated. This study then validated the FFD solvers for solving the adjoint equations and the FFD-based adjoint method for inverse identification problems and inverse designs in indoor environments. The results showed that FFD was 20 times faster than CFD in predicting transient indoor airflow, and similar computational accuracy could be maintained; the FFD-based adjoint method was 4-16 times faster than the CFD-based adjoint method in the inverse design process.

Keywords: Fast fluid dynamics; Pressure-correction schemes; Adjoint method; Inverse design

1 Introduction

To create the desired indoor environment, a good approach is to use an inverse design method to find the optimal design variables. According to Liu et al. (2015a), the computational fluid dynamics (CFD)-based genetic algorithm (Miller and Goldberg, 1995; Xue et al., 2013), CFD-based adjoint method (Liu and Chen, 2015), and proper orthogonal decomposition (POD) analysis (Li et al., 2013) can be used for such a purpose. Since POD analysis is a reduced-order model, its computing speed is the fastest, but the computational accuracy is not very good. The

other two methods directly solve the Navier-Stokes equations with a suitable turbulence model for the design objective, and thus their accuracy is high. The genetic algorithm is a gradient-free optimization method that emphasizes probability and can identify the global optima. In contrast, the adjoint method is a gradient-based optimization method that computes the gradient of design objectives over the design variables; it can identify only the local optima. However, the adjoint method can converge tens of times faster than the genetic algorithm (Liu et al., 2016a). Therefore, the CFD-based adjoint method may be appropriate for the inverse design of the indoor environment when both accuracy and efficiency are considered.

Inverse design by means of the CFD-based adjoint method requires tens of design cycles (Jameson, 1995). In each design cycle, this method solves the Navier-Stokes equations and adjoint equations in sequence by the SIMPLE (Semi-Implicit Method for Pressure-Linked Equations) algorithm (Patankar and Spalding, 1972). Therefore, a single design requires tens of Reynolds-averaged Navier-Stokes (RANS) simulations. To design an office environment, the CFD simulation normally requires mesh with 0.5 million cells, and the computing time for a single RANS simulation is about two hours with the use of a personal computer. Therefore, the inverse design process still takes at least tens of hours. For a larger indoor space such as an aircraft cabin, this method requires a powerful computer that can handle mesh with large grid number, and the computing time can be very long (Lin et al., 2005).

A method is desired that is more efficient and that can solve the Navier-Stokes/adjoint equations as accurately and informatively as does CFD simulation with the SIMPLE algorithm. A good option for solving the Navier-Stokes equations is fast fluid dynamics (FFD), which applies a time-advancement scheme and a semi-Lagrangian (SL) scheme (Staniforth and Côté, 1991). After a major development by Stam (1999) in the area of computer games, FFD has been further developed for simulating indoor airflow (Zuo and Chen, 2009; Jin et al., 2012; Liu et al., 2016b; Xue et al., 2016). These efforts have made FFD a viable alternative to CFD for simulating indoor airflow, achieving similar accuracy with low computing time or computational capacity. However, the current FFD solvers consider the airflow to be laminar, which is not true for indoor environments. Furthermore, a turbulence model cannot be directly integrated with FFD because the SL scheme in FFD introduces significant numerical viscosity. Therefore, the integration of FFD with a turbulence model requires further investigation.

Because the adjoint equations have a similar form to that of the Navier-Stokes equations, they can be solved in the same way. Othmer et al. (2007) applied the SIMPLE-type algorithm to solve the adjoint equations for shape optimization. Our previous study (Liu and Chen, 2015) also used the SIMPLE-type algorithm to solve the adjoint equations for the inverse design of an indoor environment. Although the algorithm has proven to be robust, its computational demand is the same as that for solving the Navier-Stokes equations by the SIMPLE algorithm. However, if FFD were further improved and could solve the Navier-Stokes equations fast and accurately, it is quite possible that the FFD models could be used to solve the adjoint equations.

Therefore, this study developed an FFD technique with a turbulence model to achieve fast and accurate simulation of the air distributions in an indoor environment. The FFD models were further developed to solve the adjoint equations. This study implemented the FFD solvers for

solving Navier-Stokes/adjoint equations in an open-source CFD program, OpenFOAM (Open Field Operation and Manipulation) (2007), and this paper describes the validation for indoor airflow predictions and inverse identification problems with experimental air-distribution data from the literature and the inverse design of indoor environment.

2. CFD-based adjoint method

The design of an indoor environment by the adjoint method requires an objective function $O(\boldsymbol{\xi})$ to describe the design objective. The objective function can be a function of air velocity $\mathbf{U} = (U_1, U_2, U_3)^{\mathrm{T}}$ (vector), air temperature T, etc.:

$$O(\boldsymbol{\xi}) = \int_{\Omega} f(\mathbf{U}, T) d\Omega \tag{1}$$

where $\boldsymbol{\xi}$ is a vector that represents the design variables (e.g., supply air velocity and temperature) and Ω is the design domain. The objective function is constructed so that the design objective is to identify the $\boldsymbol{\xi}$ that minimizes the function.

The CFD-based adjoint method calculates the gradient $dO/d\boldsymbol{\xi}$ for determining the direction in which to adjust $\boldsymbol{\xi}$ in order to minimize $O(\boldsymbol{\xi})$. Since the relationship between O and $\boldsymbol{\xi}$ is constrained by the Navier-Stokes equations, the gradient $dO/d\boldsymbol{\xi}$ cannot be directly computed. The Navier-Stokes equations for incompressible Newtonian flow are:

$$N_1 = -\frac{\partial U_i}{\partial x_i} = 0 \tag{2}$$

$$N_{i+1} = \frac{\partial U_i}{\partial t} + U_j \frac{\partial U_i}{\partial x_j} + \frac{1}{\rho}\frac{\partial p}{\partial x_i} - \nu \frac{\partial^2 U_i}{\partial x_j \partial x_j} - \frac{1}{\rho} F_i = 0 \tag{3}$$

$$N_5 = \frac{\partial T}{\partial t} + U_j \frac{\partial T}{\partial x_j} - \kappa \frac{\partial^2 T}{\partial x_j \partial x_j} - S_T = 0 \tag{4}$$

where $\mathbf{N}(\boldsymbol{\chi}) = (N_1, N_2, N_3, N_4, N_5)^{\mathrm{T}}$ are the Navier-Stokes equations in vector form; $\boldsymbol{\chi} = (p, \mathbf{U}, T)$ the state variables; $i, j = 1, 2$, and 3; U_i the i^{th} component of the velocity vector; p the pressure, ρ the density; F_i the i^{th} component of the body forces; ν the effective viscosity; κ the effective thermal conductivity; and S_T the energy source. To make the gradient $dO/d\boldsymbol{\xi}$ computable, the adjoint method introduces a Lagrangian multiplier $\boldsymbol{\chi}_{\mathbf{a}} = (p_a, \mathbf{U}_{\mathbf{a}}, \mathrm{T_a})$ to produce an augmented objective function as follows:

$$L(\boldsymbol{\xi}) = O(\boldsymbol{\xi}) + \int_{\Theta} \boldsymbol{\chi}_{\mathbf{a}} \cdot \mathbf{N} d\Theta \tag{5}$$

where Θ represents the computational domain and $\boldsymbol{\chi}_\mathbf{a}$ the adjoint variables. This mathematical manipulation transforms min $O(\boldsymbol{\xi})$ to min $L(\boldsymbol{\xi})$. This is because the minimum of $L(\boldsymbol{\xi})$ should satisfy:

$$\frac{\partial L}{\partial \boldsymbol{\chi}_\mathbf{a}} = 0 \rightarrow \mathbf{N} = 0 \tag{6}$$

$$\frac{\partial L}{\partial \boldsymbol{\chi}} = 0 \rightarrow \frac{\partial O}{\partial \boldsymbol{\chi}} + \int_{\Theta} \boldsymbol{\chi}_\mathbf{a} \cdot \frac{\partial \mathbf{N}}{\partial \boldsymbol{\chi}} d\Theta = 0 \tag{7}$$

$$\frac{\partial L}{\partial \boldsymbol{\xi}} = \frac{\partial O}{\partial \boldsymbol{\xi}} + \int_{\Theta} \boldsymbol{\chi}_\mathbf{a} \cdot \frac{\partial \mathbf{N}}{\partial \boldsymbol{\xi}} d\Theta = 0 \tag{8}$$

Eq. (6) represents the Navier-Stokes equations, while Eq. (7) represents the adjoint equations; the corresponding final form is:

$$\frac{\partial U_{a,i}}{\partial x_i} = 0 \tag{9}$$

$$\frac{\partial U_{a,i}}{\partial t} - U_j \frac{\partial U_{a,i}}{\partial x_j} = -\frac{\partial p_a}{\partial x_i} + \nu \frac{\partial^2 U_{a,i}}{\partial x_j \partial x_j} + F_{a,i} \tag{10}$$

$$\frac{\partial T_a}{\partial t} - U_j \frac{\partial T_a}{\partial x_j} = \kappa \frac{\partial^2 T_a}{\partial x_j \partial x_j} - \frac{\partial f}{\partial T} \tag{11}$$

where

$$F_{a,i} = \frac{\partial U_{a,j}}{\partial x_i} U_j - T_a \frac{\partial T}{\partial x_i} - \frac{\partial f}{\partial U_i} \tag{12}$$

Eq. (8) is used to compute the gradient $\partial L/\partial \boldsymbol{\xi}$. The adjoint method solves Eqs. (6), (7), and (8) in sequence. With an initialized $\boldsymbol{\xi}$, Eq. (6) is solved first to obtain $\boldsymbol{\chi}$ and calculate $O(\boldsymbol{\xi})$. The variables in Eq. (7) other than $\boldsymbol{\chi}_\mathbf{a}$ can then be obtained. In the following step, the adjoint equations (Eq. (7)) are solved to obtain $\boldsymbol{\chi}_\mathbf{a}$. Afterwards, with the use of the simple steepest descent algorithm (Bryson, 1975), the design variables can be adjusted by:

$$\boldsymbol{\xi}_{new} = \boldsymbol{\xi}_{old} - \lambda [\frac{\partial L}{\partial \boldsymbol{\xi}}]^T \tag{13}$$

where λ is a positive constant. With the adjusted $\boldsymbol{\xi}$, Eqs. (6), (7), and (8) are solved again to further adjust $\boldsymbol{\xi}$. The procedure for obtaining a new $\boldsymbol{\xi}$ is called one design cycle, and it is repeated until $O(\boldsymbol{\xi})$ is minimized. The following section introduces the FFD models that were used to solve the Navier-Stokes equations and adjoint equations.

3. Fast fluid dynamics

3.1 FFD to solve the Navier-Stokes equations

FFD solves the Navier-*S*tokes equations in a similar manner to CFD. Previous FFD models used the non-incremental pressure-correction scheme with the SL scheme (NIPC-SL) to solve the Navier-Stokes equations (Zuo and Chen, 2009). The SL scheme stabilizes the calculations for a large time step size, but it introduces extra numerical diffusion that is dependent on the time step size (Zuo et al., 2010). The numerical diffusion could be treated as the substitution of turbulent diffusion, but its significance is not controllable. It is thus necessary to employ a turbulence model for simulating real indoor airflow. However, it is quite possible that the effective diffusion would be overestimated. Therefore, this study also investigated three pressure-correction schemes without the SL scheme: the non-incremental pressure-correction (NIPC) scheme, standard incremental pressure-correction (SIPC) scheme, and rotational incremental pressure-correction (RIPC) scheme. The following section introduces the NIPC, SIPC, RIPC, and NIPC-SL in sequence.

3.1.1 Non-incremental pressure-correction scheme

The NIPC scheme is the simplest pressure-correction scheme and was originally proposed by Chorin (1968) and Temam (1969). It applies a two-step time-advancement scheme that splits the momentum equation (Eq. (3)) into two discretized equations:

$$\frac{U_i^* - U_i^n}{\Delta t} = -U_j^n \frac{\partial U_i^*}{\partial x_j} + \nu \frac{\partial^2 U_i^*}{\partial x_j \partial x_j} + \frac{1}{\rho} F_i \tag{14}$$

$$\frac{U_i^{n+1} - U_i^*}{\Delta t} = -\frac{1}{\rho} \frac{\partial p}{\partial x_i} \tag{15}$$

where U^n and U^{n+1} represent the air velocity at the previous and current time steps, respectively. U^* is the intermediate air velocity. To resolve the coupled pressure and velocity, the scheme uses the pressure projection method (Chorin, 1967), which substitutes Eq. (15) into Eq. (2) to produce:

$$\frac{\partial^2 p}{\partial x_i \partial x_i} = \frac{\rho}{\Delta t} \frac{\partial U_i^*}{\partial x_i} \tag{16}$$

The NIPC scheme first solves Eq. (14) with the implicit Euler scheme for the temporal term; the semi-implicit scheme for the convection term; and the implicit scheme for the diffusion term to obtain intermediate velocity U^*. Next, the NIPC scheme solves the Poisson equation, Eq. (16), to obtain the pressure p. Finally, the scheme calculates the air velocity at the next step U^{n+1} by solving Eq. (15) as follows:

$$U_i^{n+1} = U_i^* - \frac{\Delta t}{\rho}\frac{\partial p}{\partial x_i} \tag{17}$$

3.1.2 Standard incremental pressure-correction scheme

As observed by Goda (1979), the pressure term is missing in Eq. (14), and adding the pressure gradient of the previous step would increase the accuracy. Then the two discretized equations for the momentum equations are:

$$\frac{U_i^* - U_i^n}{\Delta t} = -\frac{1}{\rho}\frac{\partial p^n}{\partial x_i} - U_j^n\frac{\partial U_i^*}{\partial x_j} + \nu\frac{\partial^2 U_i^*}{\partial x_j \partial x_j} + \frac{1}{\rho}F_i \tag{18}$$

$$\frac{U_i^{n+1} - U_i^*}{\Delta t} = -\frac{1}{\rho}\frac{\partial (p^{n+1} - p^n)}{\partial x_i} \tag{19}$$

where p^n and p^{n+1} represent the air pressure at the previous and current time steps, respectively. Using the pressure projection again, we have:

$$\frac{\partial^2 (p^{n+1} - p^n)}{\partial x_i \partial x_i} = \frac{\rho}{\Delta t}\frac{\partial U_i^*}{\partial x_i} \tag{20}$$

Like the NIPC scheme, the SIPC scheme first solves Eq. (18) with the implicit Euler scheme for the temporal term; the semi-implicit scheme for the convection term; and the implicit scheme for the diffusion term to obtain intermediate velocity U^*. The SIPC scheme then solves the Poisson equation, Eq. (20), to obtain the pressure p^{n+1}. Finally, the SIPC scheme calculates the air velocity at the next time step U^{n+1} by solving Eq. (20) as follows:

$$U_i^{n+1} = U_i^* - \frac{\Delta t}{\rho}\frac{\partial (p^{n+1} - p^n)}{\partial x_i} \tag{21}$$

3.1.3 Rotational incremental pressure-correction scheme

The SIPC scheme uses a non-physical Neumann boundary condition enforced on the pressure that is applied to the numerical boundary layer. This limits the accuracy of the scheme (Guermond et al., 2005; Timmermans et al., 1996) and slightly modifies Eq. (21), as follows:

$$\phi^{n+1} = p^{n+1} - p^n + \nu\frac{\partial U_j^*}{\partial x_j} \tag{22}$$

$$U_i^{n+1} = U_i^* - \frac{\Delta t}{\rho}\frac{\partial \phi^{n+1}}{\partial x_i} \tag{23}$$

The solving procedure is exactly the same as for the SIPC scheme.

3.1.4 Non-incremental pressure-correction scheme with semi-Lagrangian scheme

The NIPC-SL scheme applies a three-step time-advancement scheme (Ferziger and Perić., 2002) that splits the momentum equation (Eq. (3)) into three discretized equations:

$$\frac{U_i^* - U_i^n}{\Delta t} = -U_j^n \frac{\partial U_i^n}{\partial x_j} \tag{24}$$

$$\frac{U_i^{**} - U_i^*}{\Delta t} = \nu \frac{\partial^2 U_i^{**}}{\partial x_j \partial x_j} + \frac{1}{\rho} F_i \tag{25}$$

$$\frac{U_i^{n+1} - U_i^{**}}{\Delta t} = -\frac{1}{\rho} \frac{\partial p}{\partial x_i} \tag{26}$$

where U^* and U^{**} are intermediate air velocities. Using the pressure projection, we have:

$$\frac{\partial^2 p}{\partial x_i \partial x_i} = \frac{\rho}{\Delta t} \frac{\partial U_i^{**}}{\partial x_i} \tag{27}$$

The NIPC scheme with the SL scheme first solves Eq. (24) with the SL scheme to obtain intermediate air velocity U^*. Our previous study (Liu et al., 2016b) describes the SL scheme in detail. The NIPC scheme then solves the two Poisson equations, Eqs. (25) and (27), in sequence to obtain intermediate air velocity U^{**} and air pressure p, respectively. Finally, the algorithm calculates the air velocity at the next time step U^{n+1} by solving Eq. (26).

3.2 FFD to solve the adjoint equations

The adjoint equations have the same form as the Navier-Stokes equations, Eqs. (9), (10), and (11). We can apply the previously mentioned FFD methods to solve the adjoint equations. For example, applying the SIPC scheme, this study again used a two-step time-advancement scheme that splits the adjoint momentum equation (Eq. (10)) into two discretized equations:

$$\frac{U_{a,i}^* - U_{a,i}^n}{\Delta t} = -\frac{\partial p_a}{\partial x_i} + U_j \frac{\partial U_{a,i}^*}{\partial x_j} + \nu \frac{\partial^2 U_{a,i}^*}{\partial x_j \partial x_j} + F_{a,i} \tag{28}$$

$$\frac{U_{a,i}^{n+1} - U_{a,i}^*}{\Delta t} = -\frac{\partial (p_a^{n+1} - p_a^n)}{\partial x_i} \tag{29}$$

where p_a^{n+1} and p_a^n represent the adjoint pressure at the previous and current time steps, respectively. U_a^* is the intermediate adjoint velocity. Using the pressure projection, we have:

$$\frac{\partial^2(p_a^{n+1}-p_a^n)}{\partial x_i \partial x_i}=\frac{1}{\Delta t}\frac{\partial U_{a,i}^*}{\partial x_i} \tag{30}$$

The SIPC scheme first solves Eq. (28) with the implicit Euler scheme for the temporal term; the semi-implicit scheme for the convection term; and the implicit scheme for the diffusion term to obtain intermediate adjoint velocity U_a^*. Next, the SIPC scheme solves the Poisson equation, Eq. (30), to obtain the adjoint pressure p_a^{n+1}. Finally, the SIPC scheme calculates the adjoint velocity at the next time step U_a^{n+1} by solving Eq. (29) as follows:

$$U_{a,i}^{n+1}=U_{a,i}^*-\Delta t\frac{\partial(p_a^{n+1}-p_a^n)}{\partial x_i} \tag{31}$$

4 Results

After developing the FFD solvers for the Navier-Stokes/adjoint equations, this study implemented them in OpenFOAM and validated their accuracy and efficiency step by step. In the first step, this investigation validated the FFD solvers for predicting steady-state and transient flow in indoor environments. Next, this study assessed the accuracy of the FFD solvers in solving the adjoint equations. Finally, this study compared the CFD-based and FFD-based adjoint methods for the inverse design of indoor environments.

4.1 FFD to predict the indoor airflow

This study used two cases with experimental data from the literature, mixed convection flow in a simplified room and an office with displacement ventilation, to test the FFD solvers in predicting steady-state and transient indoor airflow. CFD simulations with the SIMPLE algorithm were used as a reference.

4.1.1 Steady-state mixed convection flow in a simplified room

This study tested the FFD solvers with data for mixed convection flow in a simplified room from Wang and Chen (2009). Figure 1 shows a 2.44 m × 2.44 m × 2.44 m room with a plane jet from the upper left corner. The inlet height was 0.03 m. The inlet air velocity was 0.455 m/s with a corresponding Reynolds number of approximately 2,000. The supply air temperature was 22.2°C. The inlet jet developed along the ceiling and reached the far right side of the room, and then the flow moved downward because of the presence of the right-side wall, forming a circulation pattern in the room. The outlet height was 0.08 m. A box in the middle of the room, with dimensions of 1.22 m × 1.22 m × 1.22 m and a 700 W heat source inside, was used to represent a mass such as furniture or occupants. The temperatures of the box surface, ceiling, surrounding walls, and floor were 36.7, 25.8, 27.4, and 26.9 °C, respectively. The heated box formed a thermal plume, and thus the type of airflow in the room was mixed convection.

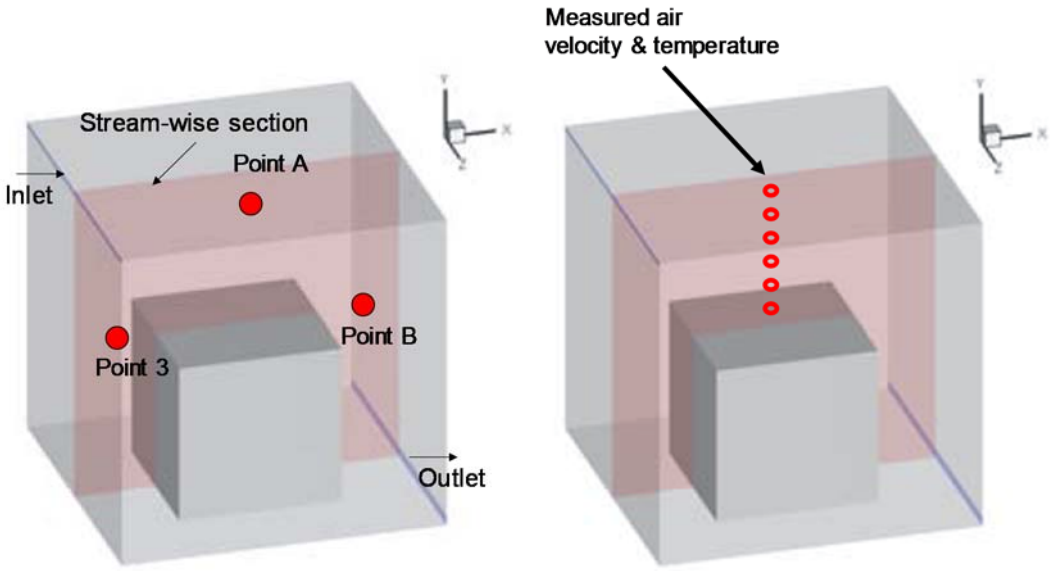

Figure 1. Sketch of the room with a box, the monitored positions, and the design objective

This investigation applied the zero equation (0-eqn) model (Chen and Xu, 1998) to simulate the turbulence, since Zhang et al. (2007) had concluded that this model performs well in predicting the mixed convection flow in an indoor environment. The turbulent viscosity was determined from the local mean air velocity |**U**| and a length that represented the shortest distance l to the wall:

$$\nu_t = 0.03874 \,|\mathbf{U}|\, l \tag{32}$$

This study compared the simulated and measured velocity distributions in Figure 2 to assess the performance of the FFD solvers. The CFD simulation used the SIMPLE algorithm, and the 0-eqn model was used as a reference. In general, the velocity distributions, except the one predicted by NIPC-SL, were very similar and agreed well with the measured distribution. The poor performance of NIPC-SL was due to the significant extra numerical diffusion that was added by the SL scheme.

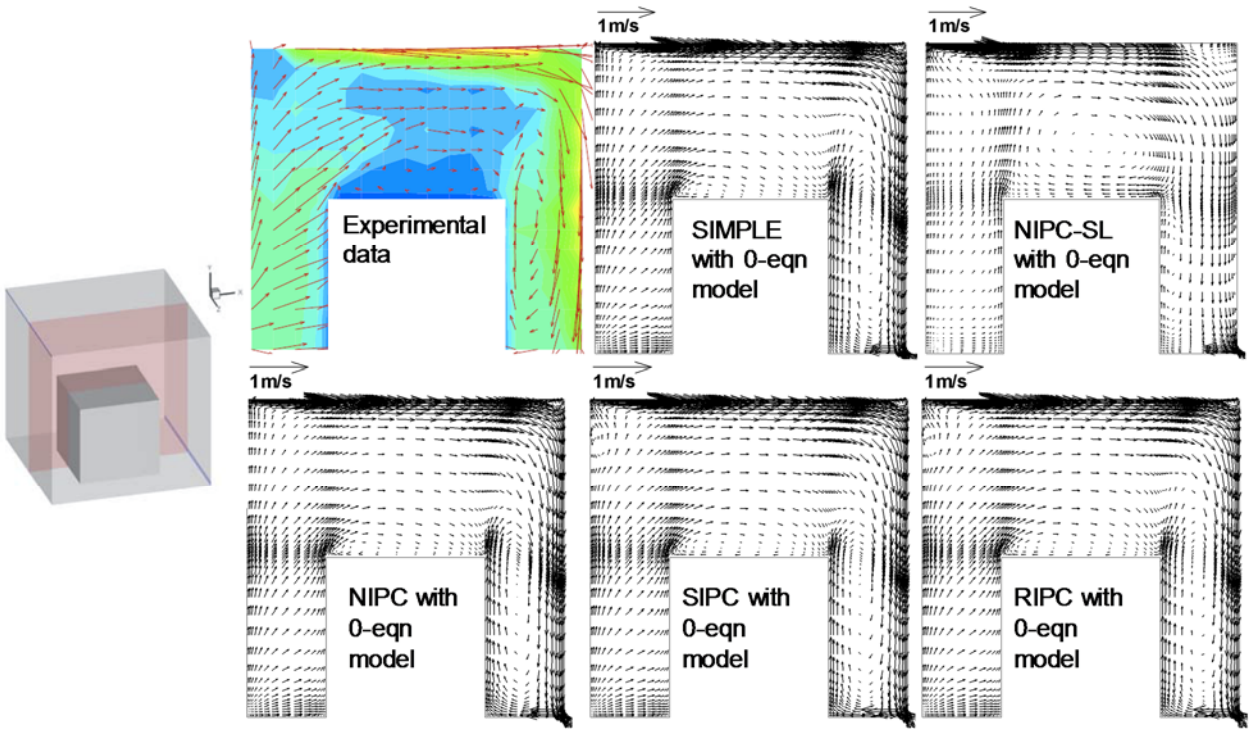

Figure 2. Airflow patterns measured by Wang and Chen (2009) and predicted by CFD and FFD with the 0-eqn model

To allow a quantitative comparison, Figure 3 shows the calculated air velocity profiles along with the measured data at four representative positions (vertical lines) in the room. These positions are in the jet upstream (position 1), in the jet downstream (position 5), at the center of the room (position 3), and at a location close to the right-side wall (position 6). The air velocity was normalized by U_{max} = 1.5 m/s. The CFD simulation used the SIMPLE algorithm, and the 0-eq model provided a fairly good prediction of the air velocity. The NIPC-SL with the 0-eqn model performed poorly, as it under-predicted the jet flow and the re-circulated flow. The NIPC, SIPC, and RIPC schemes with the 0-eqn model had very similar performance, and the predicted air velocity profiles agreed well with the experimental data. However, there was still a significant difference in the lower part of position 5. This difference occurred because the flow there was very complicated; the box and the jet interacted and generated a secondary recirculation. Wang and Chen (2009) had tried more sophisticated models such as large eddy simulation, which was not able to predict the measured velocity profile at this location either.

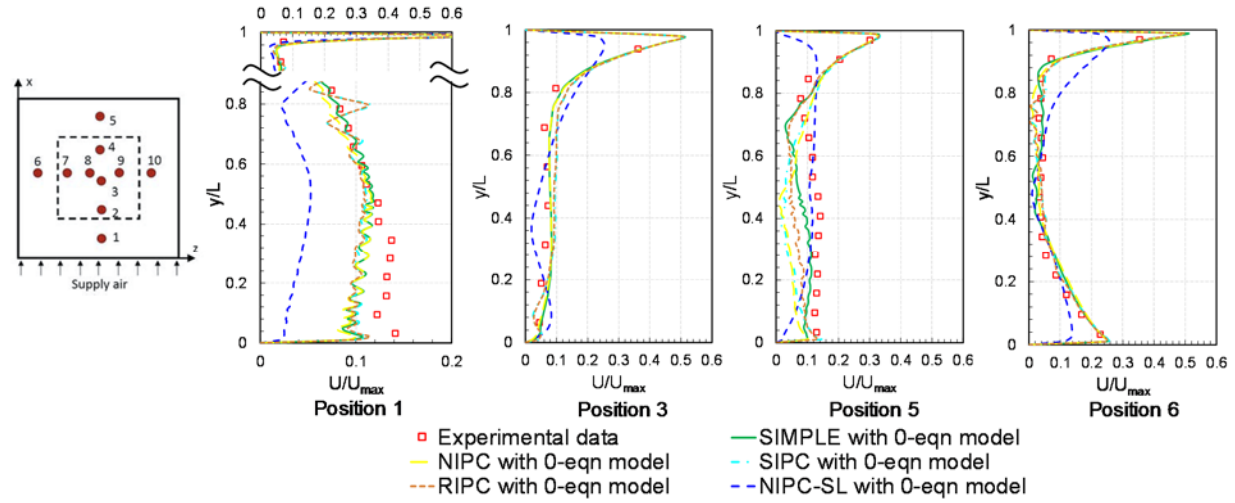

Figure 3. Comparison of air velocity profiles predicted by CFD and FFD with the 0-eqn model, with the experimental data from Wang and Chen (2009) at positions 1, 3, 5, and 6

This case was non-isothermal, and Figure 4 compares the predicted temperature profiles with the experimental data in the same positions as in Figure 3. The temperature was normalized by using T_{min} = 22.2 °C and T_{max} = 36.7 °C, which were the measured minimum and maximum air temperatures, respectively, in this case. All the numerical simulations of air temperature agreed well with the experimental data.

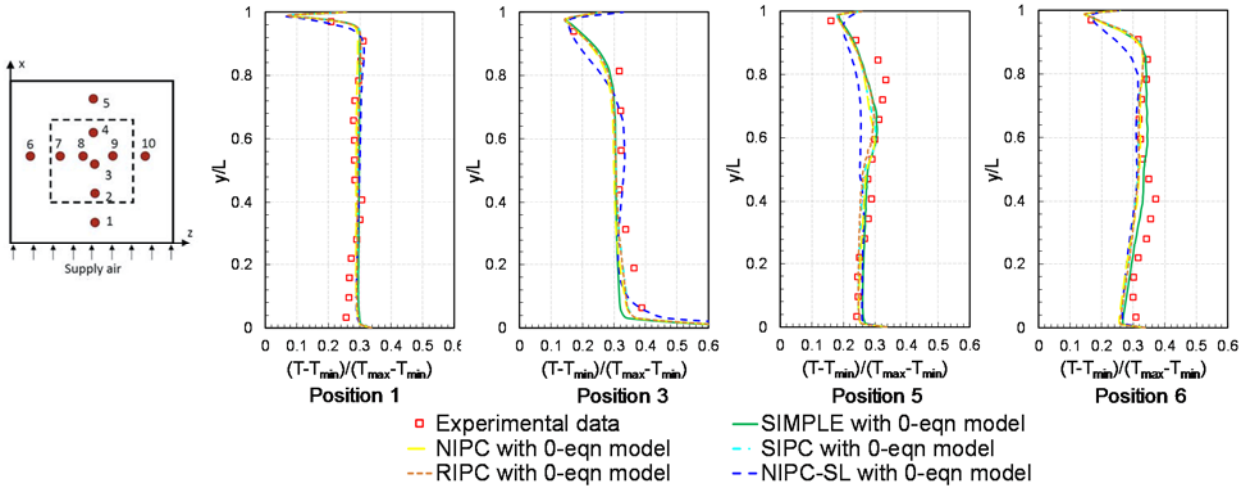

Figure 4. Comparison of air temperature profiles predicted by CFD and FFD with the 0-eqn model, with the experimental data from Wang and Chen (2009) at positions 1, 3, 5, and 6

In the above calculations, the FFD simulations with the 0-eqn model solved the transient Navier-Stokes equations with a time step size of 0.05 s for a physical flow time of 200 s, to obtain steady-state flow. The corresponding mean CFL (Courant–Friedrichs–Lewy) number was as small as 0.19, which ensured computational accuracy. To test the effect of time step size on the predictions, this study increased the step size as shown in Table 1.When Δt = 0.2 s, the corresponding mean CFL number was 0.75. To ensure that the mean CFL number was less than

1, the time step size was not further increased.

Table 1. Time step size vs. CFL number

Δt	0.05 s	0.10 s	0.20 s
CFL_{mean}	0.19	0.38	0.75
CFL_{max}	6.8	13.6	27.3

This study conducted the FFD simulations using the SIPC scheme with different time step sizes, again for a physical flow time of 200 s. Figure 5 compares the predicted air velocity profiles with the measured data at the same four representative positions in the room. At position 5, the predicted air velocity profile with Δt = 0.2 s differed somewhat from the other predictions. It must have been a coincidence that the prediction with the largest time step size had better agreement with the experimental data. Figure 6 compares the predicted profiles for air temperature with the measured data, and the predictions with different time step sizes exhibit almost no difference.

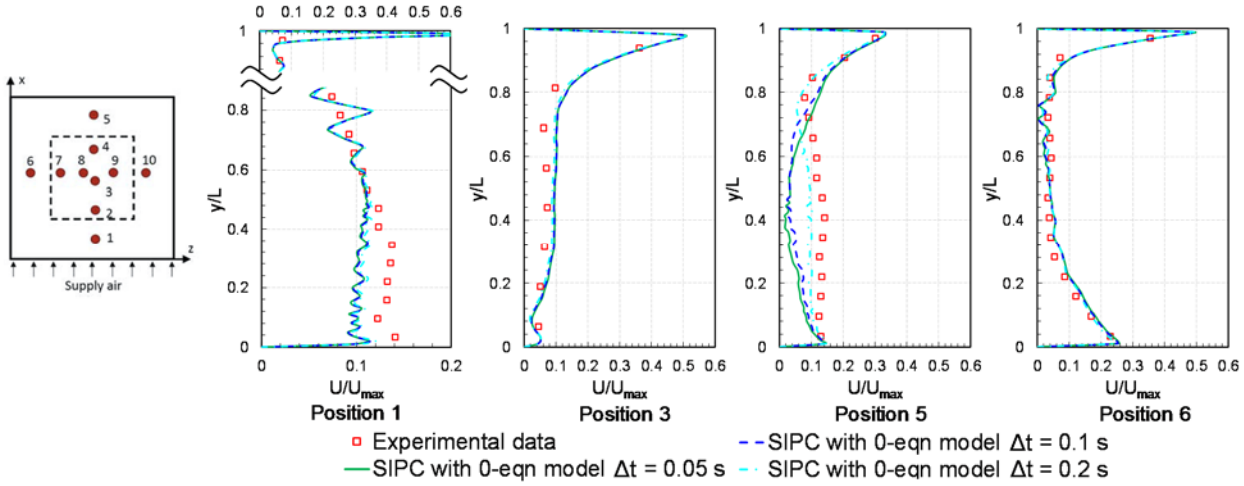

Figure 5. Comparison of air velocity profiles predicted by the SIPC scheme with the 0-eqn model, with the experimental data from Wang and Chen (2009) at positions 1, 3, 5, and 6

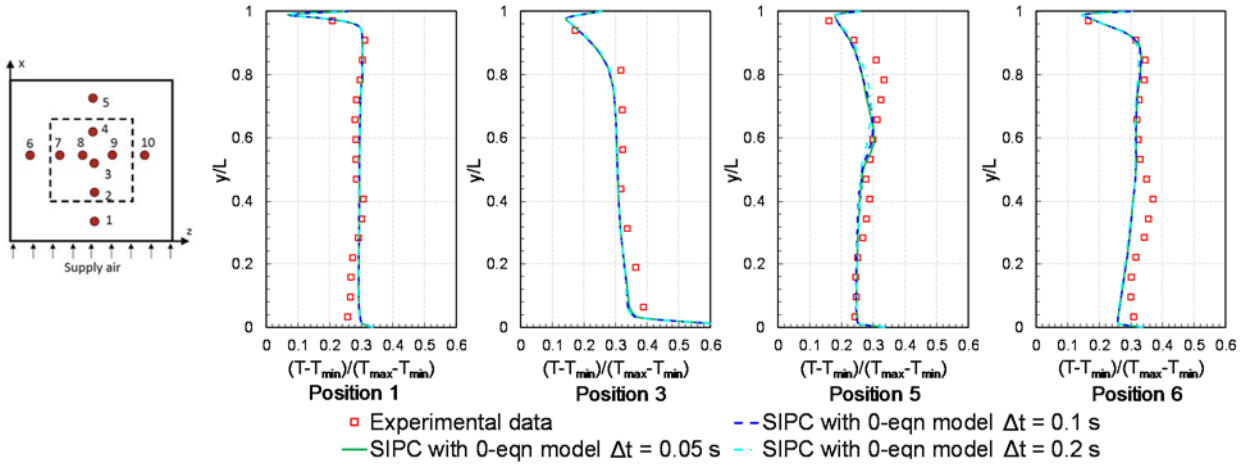

Figure 6. Comparison of air temperature profiles predicted by the SIPC scheme with the 0-eqn model, with the experimental data from Wang and Chen (2009) at positions 1, 3, 5, and 6

4.1.2 Transient mixed convection flow in a simplified room

In addition to steady-state flow, it was necessary to validate the performance of the FFD solvers in predicting transient flow in an indoor environment. Since the above-mentioned experiment by Wang and Chen (2009) did not measure the transient flow fields, this study used the airflow predicted by CFD simulation with the SIMPLE algorithm as a reference. The NIPC-SL scheme was abandoned as it could not accurately predict even the steady-state indoor airflow. To eliminate possibility of error introduced by the turbulence model, this study adopted the RNG k-ε model (Yakhot et al., 1993), which is much more sophisticated than the 0-eqn model, to simulate the turbulence. This study calculated the flow for 100 s with a time step size of 0.05 s. The initialized temperature field and flow field were uniform with T = 301.5 K and $\mathbf{U} = 0$, respectively.

This study monitored the transient air velocity and temperature at three typical locations, points A, B, and C, as shown in Figure 1. These locations were in the jet downstream, at the outlet, and in the flow recirculation area. As shown in Figure 7, the transient air velocity and temperature predicted by the FFD simulations had the same features as those predicted by the SIMPLE algorithm. There was a noticeable difference in velocity magnitude, although the difference was as small as 0.02 m/s. For the monitored air temperature, the predictions by the projection methods differed only minimally from the prediction by the SIMPLE algorithm. Overall, the SIPC and RIPC performed in a very similar manner, and their predictions were in better agreement with those predicted by SIMPLE algorithm.

Figures 8 and 9 further compare the flow fields and temperature fields in the stream-wise section (refer to Figure 1) predicted by the SIMPLE algorithm and FFD simulations at t = 5 s, 10 s, 15 s, 20 s, 25 s, and 30 s, when the flow and temperature fields changed significantly. It is clear that all the FFD simulations were as capable as the SIMPLE algorithm in capturing the flow and thermal features. At each time point, the flow and temperature fields predicted by the FFD simulations agreed well with those predicted by the SIMPLE algorithm. Both the FFD and CFD simulations were conducted with the same structured mesh on a personal computer using a single CPU core at 3.50 GHz. The computing time for the FFD simulations was 0.4 hour, and that for the CFD simulations was 7.7 hours. FFD was almost 20 times faster than CFD in predicting the transient flow, while maintaining similar prediction accuracy. We also found that the computing time for FFD simulation with the 0-eqn model was 0.32 hour, and thus the integration with the RNG k-ε model would not significantly increase the computational effort.

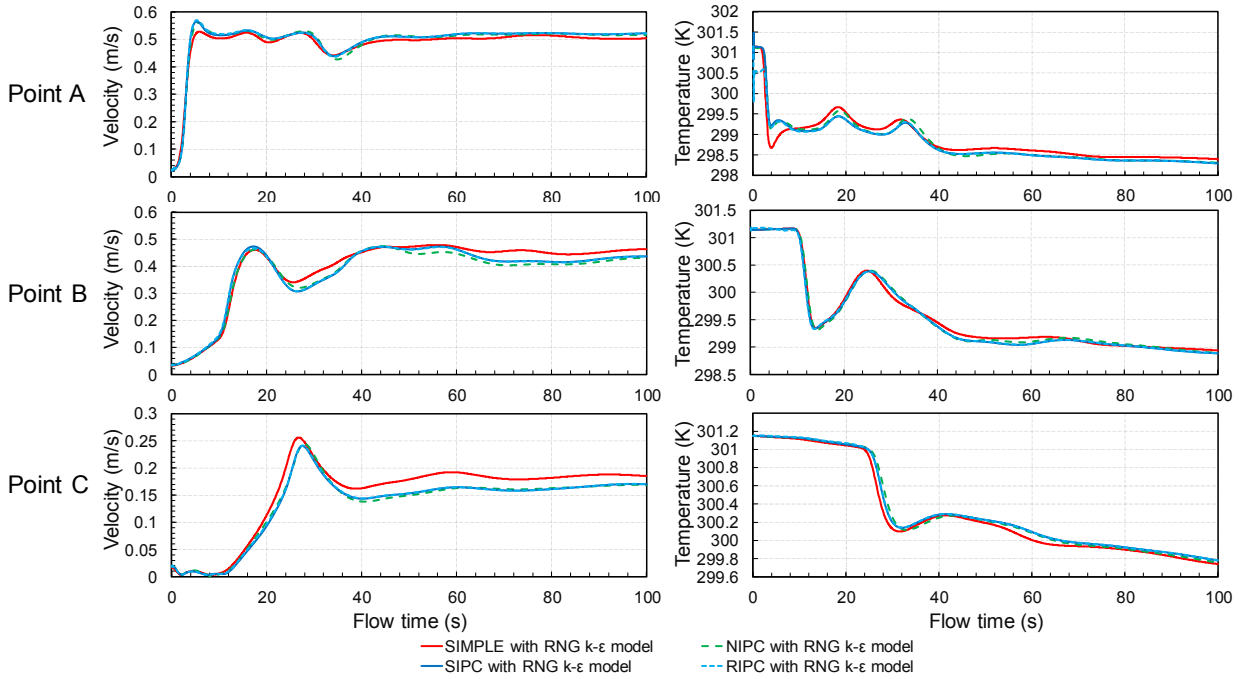

Figure 7. Monitored transient air velocity and temperature at points A, B, and C (refer to Figure 1 for the locations of the monitoring points)

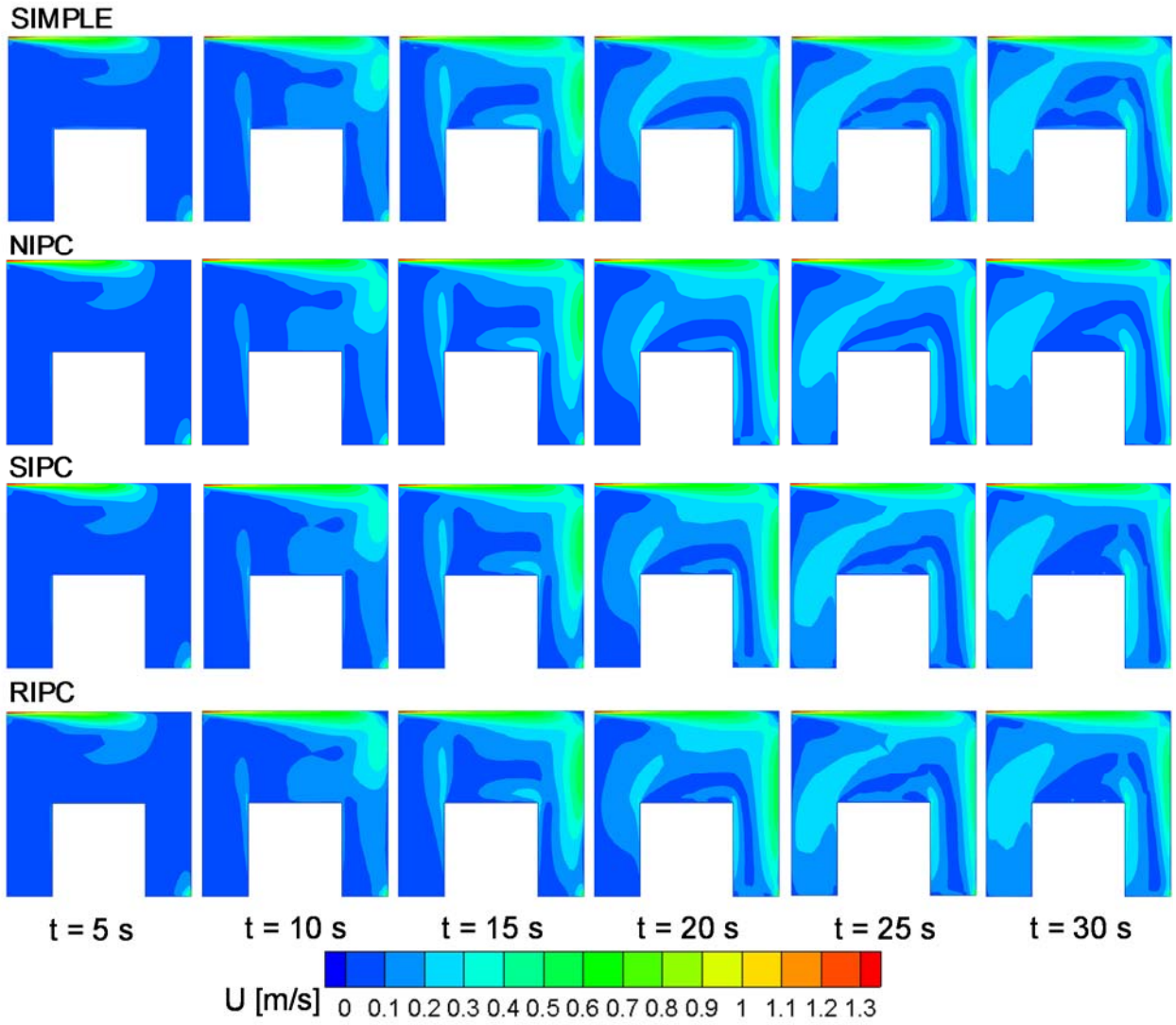

Figure 8. Predicted flow fields in the stream-wise section (refer to Figure 1) at t = 5 s, 10 s, 15 s, 20 s, 25 s, and 30 s

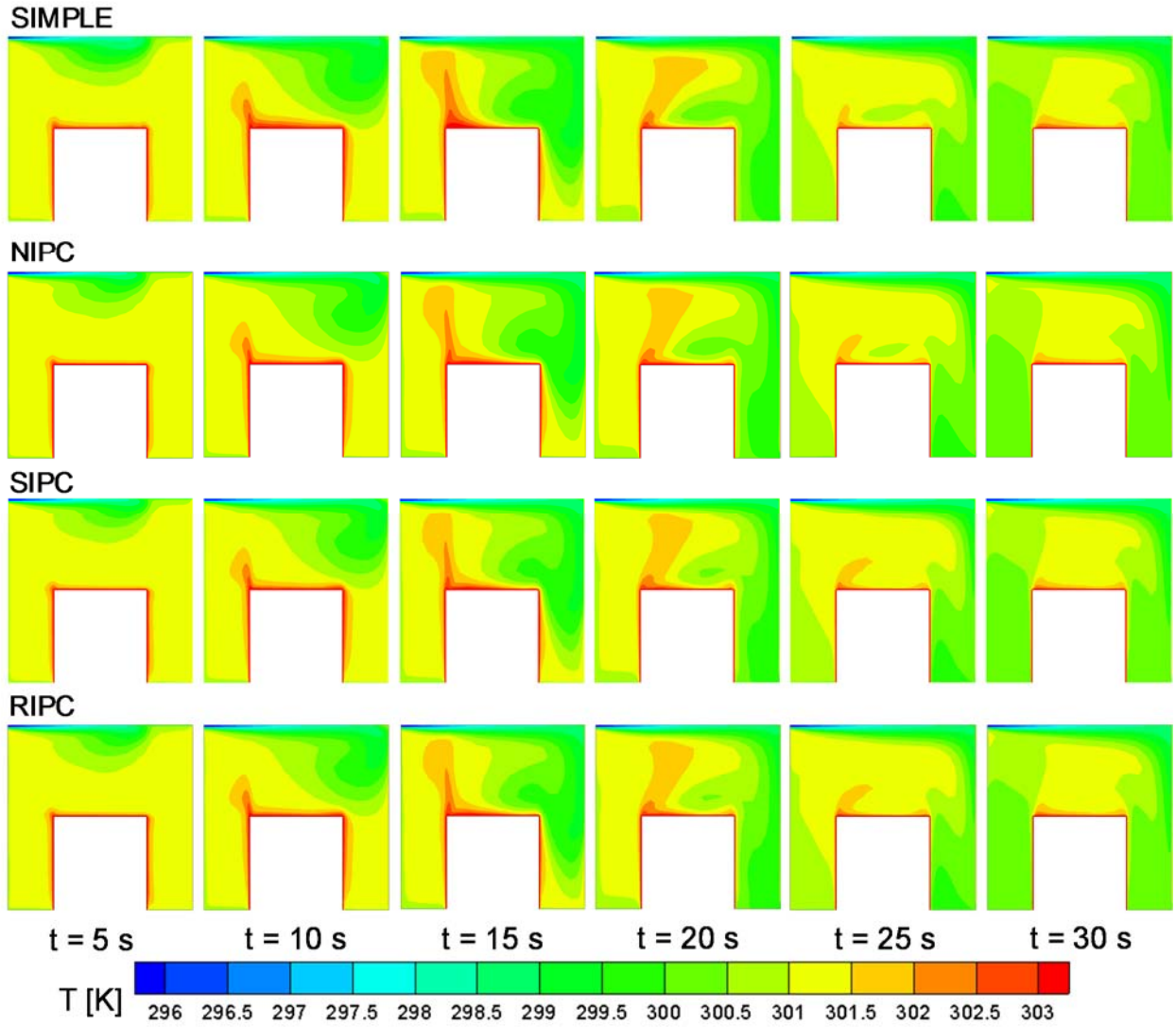

Figure 9. Predicted temperature fields in the stream-wise section (refer to Figure 1) at t = 5 s, 10 s, 15 s, 20 s, 25 s, and 30 s

For the transient airflow, this study again conducted FFD simulations using the SIPC scheme and RNG k-ε model with the various time step sizes shown in Table 1. Figures 10 and 11 show the flow fields and temperature fields on the stream-wise section predicted by the SIPC scheme at t = 5 s, 10 s, 15 s, 20 s, 25 s, and 30 s with different time step sizes. There was a noticeable difference among the predictions by various time step sizes at the beginning of the simulation (when t < 15 s). Later, as the airflow developed, the predictions were almost the same for the different time step sizes. This result agreed with the observed similarity among the predicted steady-state air distributions with different time step sizes. To further decrease the computational effort, a smaller time step size could be used at the beginning of the simulation and a larger step size later.

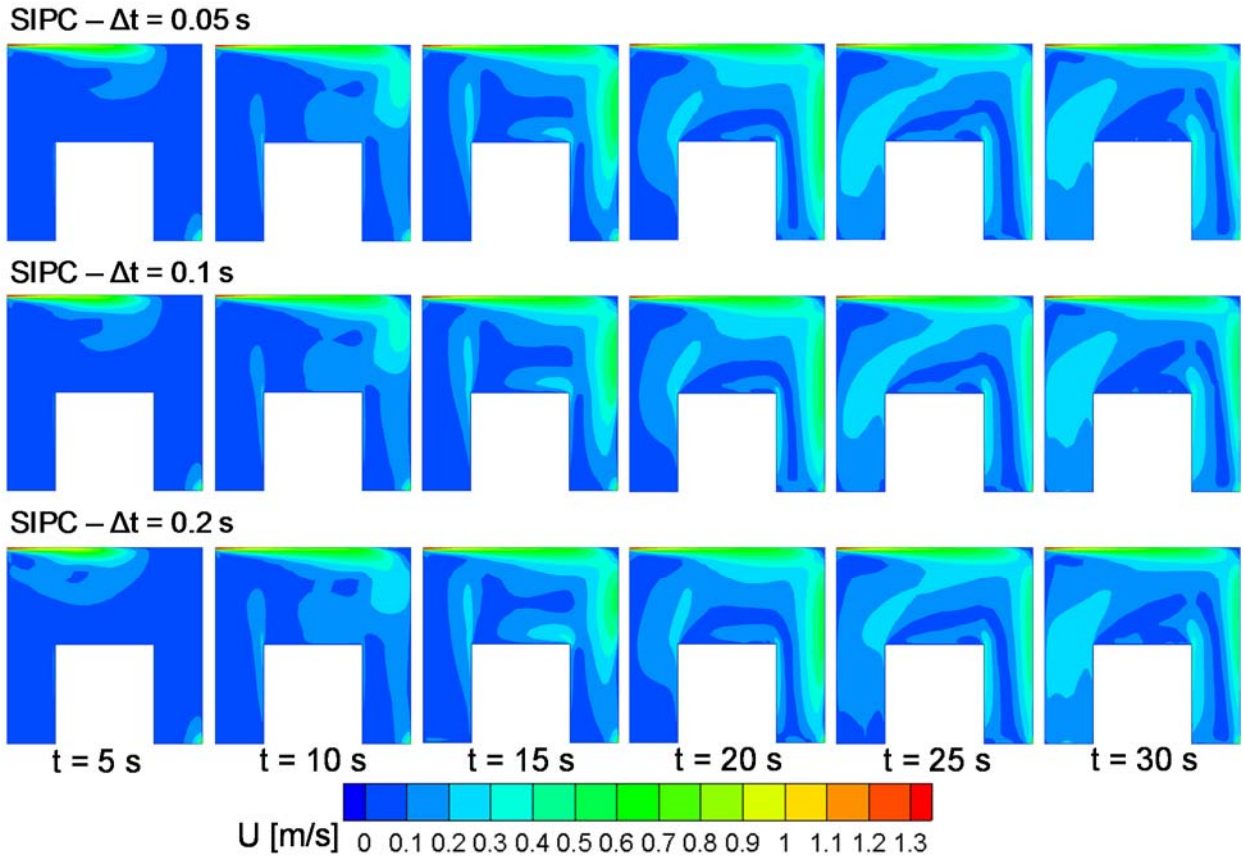

Figure 10. Flow fields predicted by the SIPC scheme with different time step sizes in the stream-wise section (refer to Figure 1) at t = 5 s, 10 s, 15 s, 20 s, 25 s, and 30 s

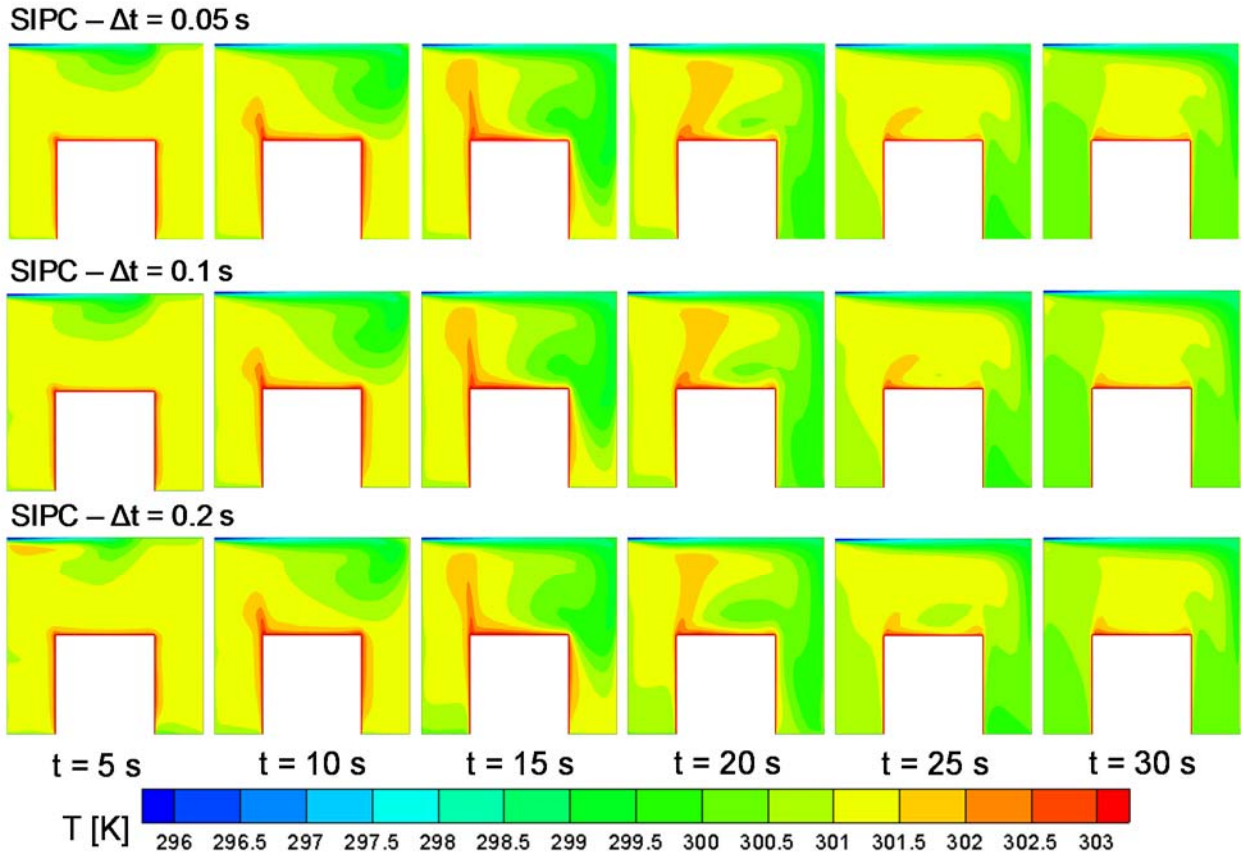

Figure 11. Temperature fields predicted by the SIPC scheme with different time step sizes in the stream-wise section (refer to Figure 1) at t = 5 s, 10 s, 15 s, 20 s, 25 s, and 30 s

4.1.3 Steady-state flow in an office with displacement ventilation

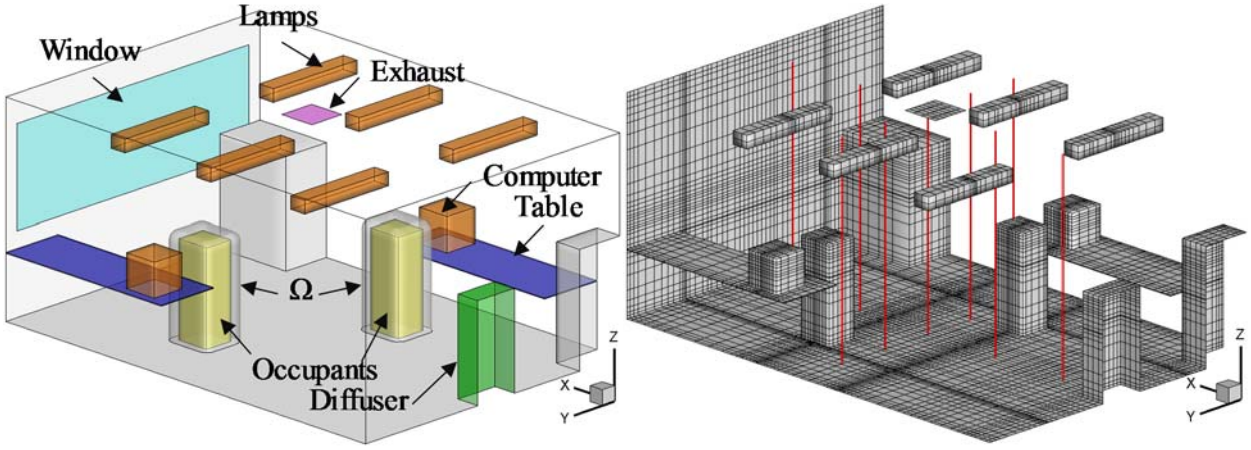

(a) (b)

Figure 12. (a) Schematic of an occupied office and (b) mesh of displacement ventilation in the office (where the red vertical lines represent measurement locations for air velocity and temperature)

This investigation also tested the FFD simulation with a more realistic indoor airflow case. Figure 12 shows an occupied office with displacement ventilation. The office was simulated by an experimental chamber of 5.16 m × 3.65 m × 2.43 m with a displacement diffuser on the side wall supplying air with a ventilation rate of four air changes per hour. The supply-air temperature was 17 °C. There were two occupants, two computers, two tables, two boxes, and six lamps in the room, as shown in Figure 12(a). For detailed sizes, locations, and heat release of these items and other thermo-fluid boundary conditions, one can refer to Yuan et al. (1999). The experiment measured the air temperature and air velocity along nine vertical poles distributed in the stream-wise center plane and the cross-sectional center plane, as indicated by the red lines in Figure 12(b). Figure 12(b) also shows the mesh that was chosen on the basis of our grid independence test.

Since this was a much more realistic case, this study used the RNG k-ε model to simulate the turbulence. Because of the poor performance of the NIPC-SL algorithm in the previous two cases, this study did not consider it for this case. The CFD simulation with the SIMPLE algorithm was again used as a reference.

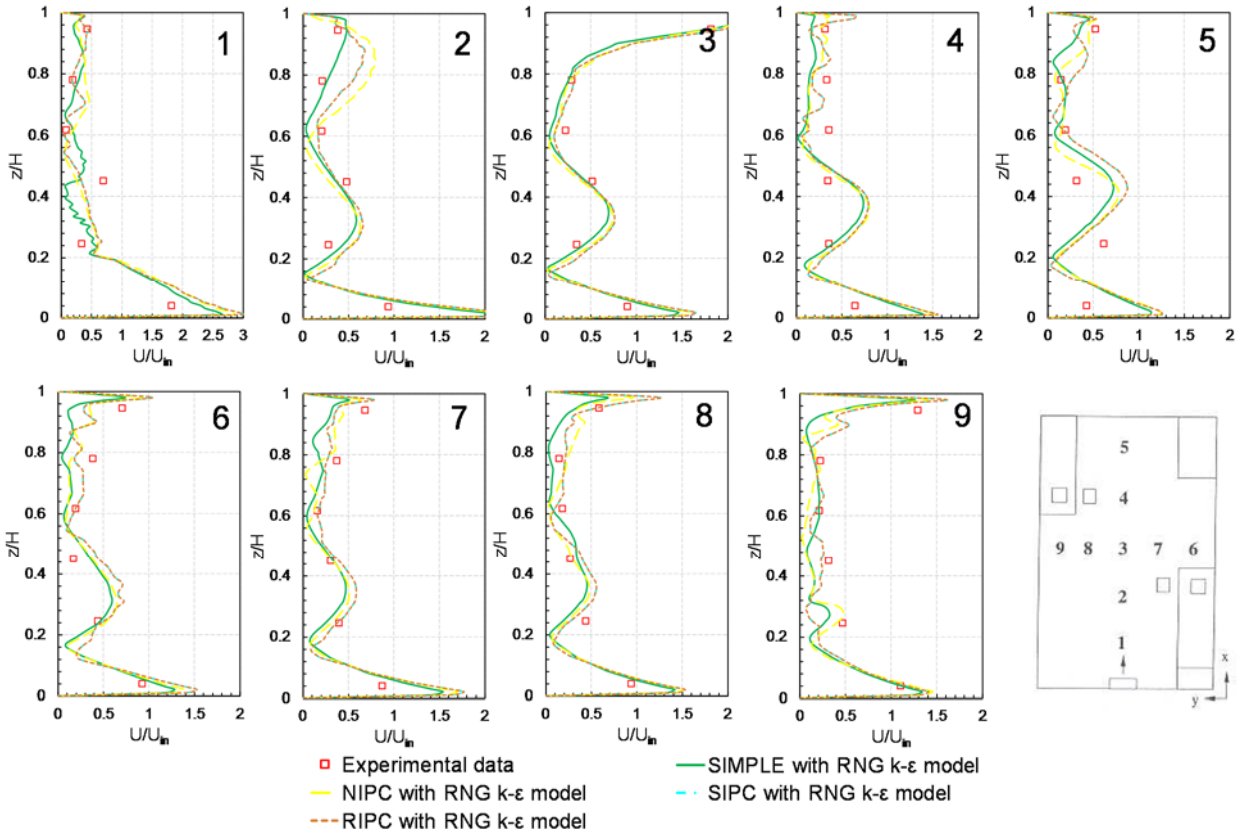

Figure 13. Comparison of air velocity profiles predicted by CFD and FFD with the RNG k-ε model, with the experimental data from Yuan et al. (1999)

This study compared the calculated air velocity profiles with the measured data at the nine

positions in the room, as shown in Figure 13. The air velocity was normalized by the inlet air velocity U_{in} = 0.09 m/s. There was good quantitative agreement between the predicted and measured air velocity. All the FFD simulations had almost the same performance, and it was hard to determine whether the SIMPLE algorithm or the FFD models performed better. Figure 14 compares the calculated profiles for air temperature with the measured data at the nine positions in the room. The normalized air temperature θ was defined as $(T - T_s)/(T_r - T_s)$, where T_s (supply air temperature) = 17.0 °C and T_r (return air temperature) = 26.7 °C. Again, the quantitative agreement between the predicted and measured air temperature was good. Thus, the FFD simulations without the SL scheme performed no worse than the SIMPLE algorithm in predicting steady-state flow in this indoor environment.

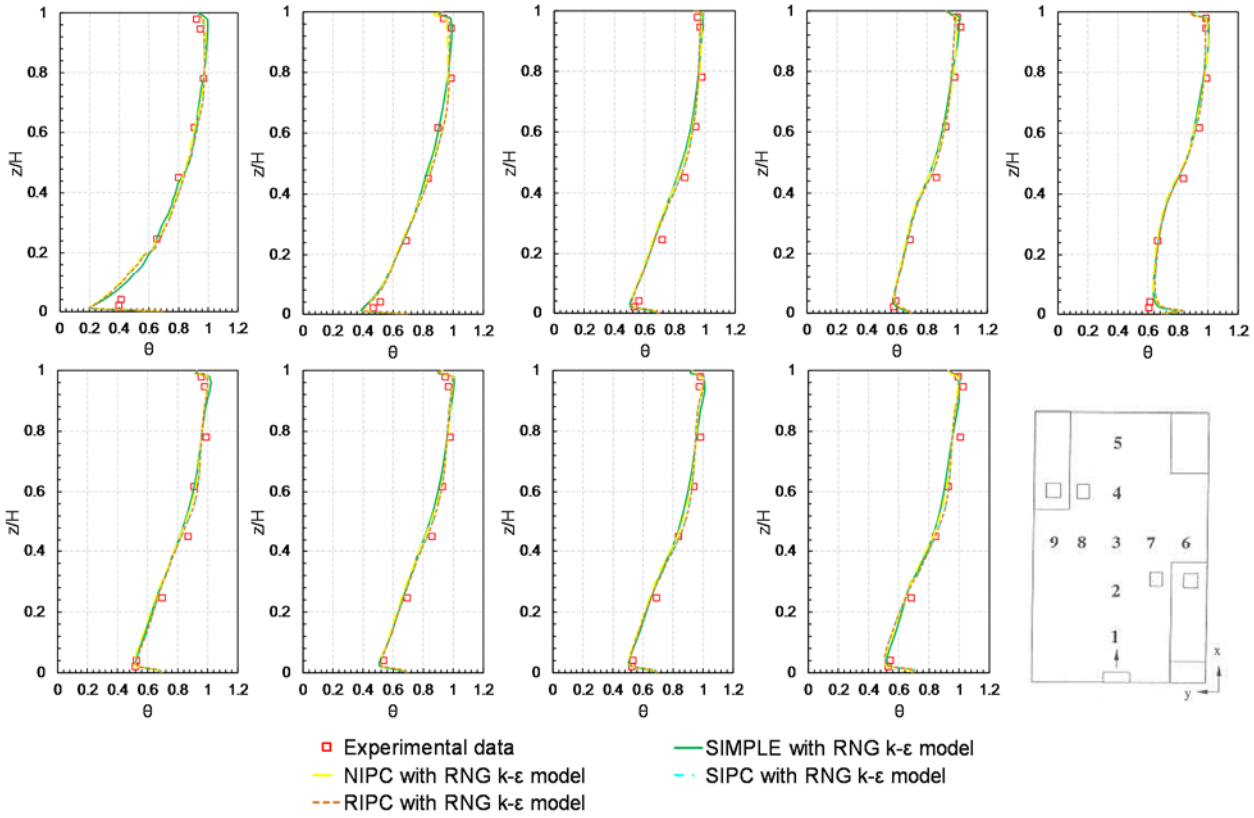

Figure 14. Comparison of air temperature profiles predicted by CFD and FFD with the RNG k-ε model, with the experimental data from Yuan et al. (1999)

4.2 FFD to solve the adjoint equations

To validate the accuracy of FFD in solving the adjoint equations, this study compared the adjoint velocity fields predicted by the SIMPLE algorithm and SIPC scheme in the first design cycle of an inverse identification problem. The goal of this problem was to inversely identify the air supply velocity by setting the measured air velocity as the design objective. Figure 15 shows a two-dimensional, non-isothermal case with experimental data from Blay et al. (1992). The dimensions of the flow domain were H × H = 1.04 m × 1.04 m, the inlet height was h_{in} = 18 mm, and the outlet height was h_{out} = 24 mm. In the experiment, the inlet air velocity was U_x = 0.57

m/s, U_y = 0.0 m/s, and the inlet air temperature (T_{in}) was 15 ºC. The temperature of the walls (T_{wl}) was 15 ºC, and that of the floor (T_{fl}) was 35.5 ºC, in order to create a thermal plume. The measured air velocity on the red dashed line was set as the design objective, and thus the objective function is:

$$O(\mathbf{U}_{in}) = \int_{\Omega} |\mathbf{U} - \mathbf{U}_0|^2 \, d\Omega \tag{33}$$

where $\mathbf{U_0}$ is the measured air velocity.

In the inverse identification of the air supply velocity, this study applied the SIMPLE algorithm and SIPC scheme to solve the Navier-Stokes and adjoint equations, respectively. The SIMPLE algorithm solved the steady-state Navier-Stokes/adjoint equations for 7,000 iterations to ensure convergence. The SIPC scheme solved the transient Navier-Stokes/adjoint equations for 100 s with a time step size of 0.05 s in each design cycle. The RNG k-ε model was adopted to simulate the turbulence. The initialized air supply velocity was **U** = (1.0, 0.2) m/s.

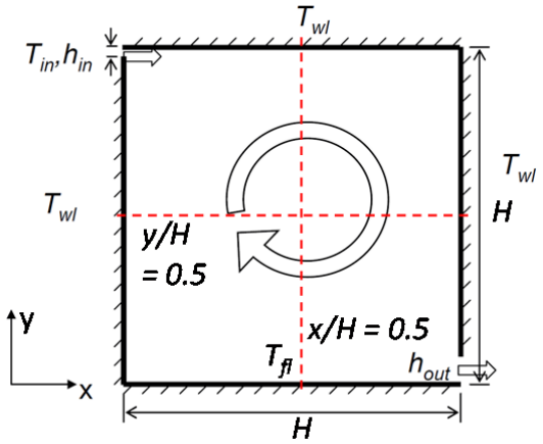

Figure 15. Sketch of the two-dimensional, non-isothermal case

Figure 16 compares the air flow fields, temperature fields, and adjoint velocity fields predicted by the SIMPLE algorithm and SIPC scheme in the first design cycle. With the same initialized air supply velocity, the predicted flow fields and temperature fields were almost the same. The two adjoint velocity fields had very similar features, and the field predicted by SIPC had a slightly larger $\mathbf{U_a}$ magnitude. If the adjoint velocity field predicted by the SIMPLE algorithm is reliable, then it is clear that the SIPC scheme performs well in solving the adjoint equations.

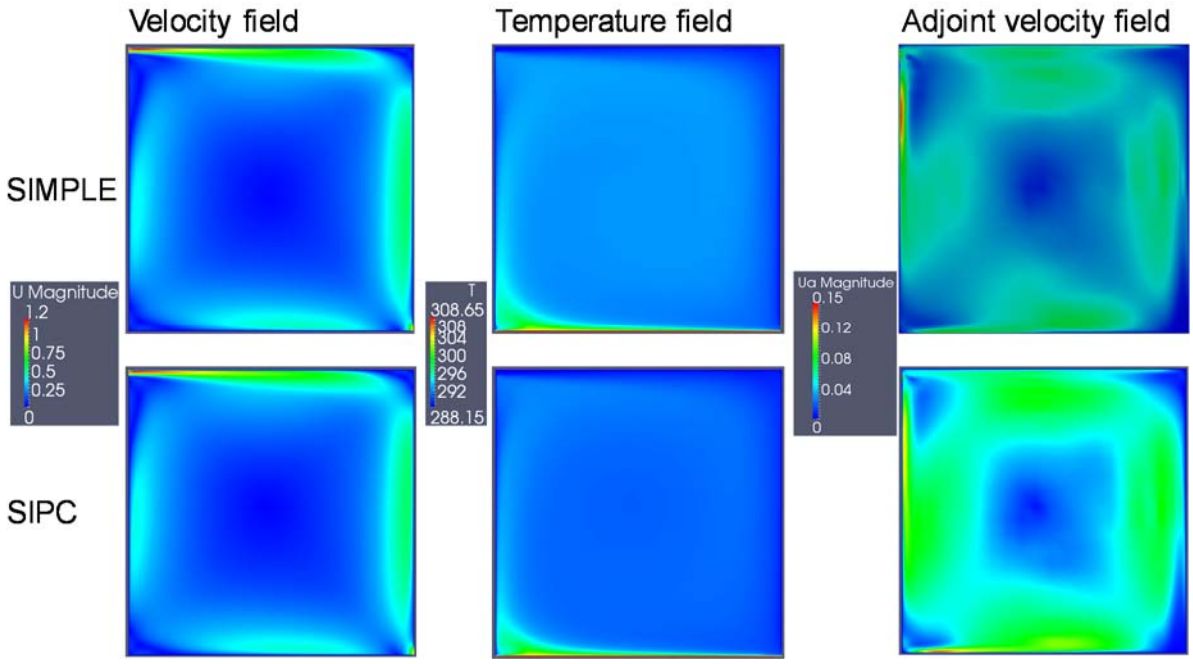

Figure 16. Air flow fields, temperature fields, and adjoint velocity fields predicted by the SIMPLE algorithm and SIPC scheme in the first design cycle

4.3 FFD-based adjoint method vs. CFD-based adjoint method

The previous two sections discussed the validation of the FFD for solving the Navier-Stokes equations and adjoint equations. The present section compares the FFD-based adjoint method and CFD-based adjoint method in two inverse identification cases and one inverse design case.

4.3.1 Inverse identification of air supply velocity in a 2D cavity

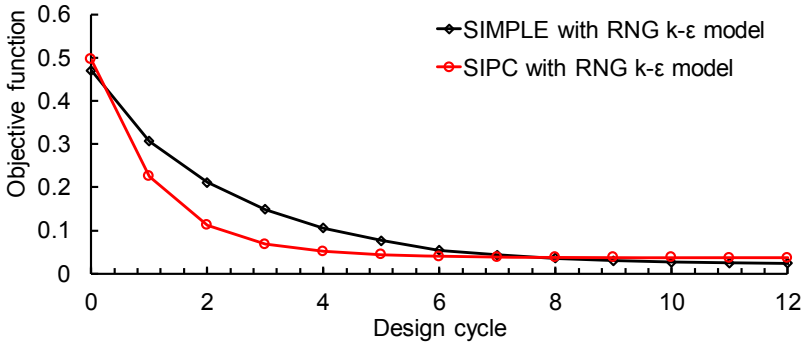

Figure 17. Objective function versus design cycle

This study applied the FFD-based adjoint method and CFD-based adjoint method for the inverse identification of the air supply velocity in Section 4.2. The FFD-based adjoint method used the SIPC scheme, and the CFD-based adjoint method used the SIMPLE algorithm. One can refer to Section 4.2 for other parameters. The convergence criterion for the inverse identification was

$|O_{new} - O_{old}| < 0.001$. Figure 17 shows the objective function versus the design cycle. Both methods led the objective to very small values, and both inverse identifications converged. The convergence speed differed because of the difference in the predicted adjoint fields. In one design cycle, this study found that the SIPC scheme was four times faster than the SIMPLE algorithm.

4.3.2 Inverse identification of air supply conditions in a simplified room

To further validate the FFD-based adjoint method for the inverse design process, this study attempted to inversely identify the air supply velocity and temperature in a simplified room as shown in Figure 1. The measured air velocity and temperature at the points indicated by the red circles in the figure were set as the design objective. Therefore, the objective function is:

$$O(\mathbf{U}_{in}, T_{in}) = \frac{1}{|\mathbf{U}_{\max}|^2}\int_{\theta} |\mathbf{U} - \mathbf{U}_0|^2 \, d\theta + \frac{1}{(T_{\max} - T_{\min})^2}\int_{\theta} (T - T_0)^2 \, d\theta \tag{34}$$

The FFD-based adjoint method again used the SIPC scheme. This scheme solved the transient Navier-Stokes/adjoint equations for 100 s with time step sizes of 0.05 s, 0.1 s, and 0.2 s. Inverse identification by means of the CFD-based adjoint method was used as a reference. The SIMPLE algorithm solved the steady-state Navier-Stokes/adjoint equations for 5,000 iterations to ensure convergence. The RNG k-ε model was adopted to simulate the turbulence. Since the air supply velocity and temperature in the experiment were $\mathbf{U_{in}}$ = (1.366, 0, 0) m/s and T_{in} = 295.35 K, respectively, this study initialized them as $\mathbf{U_{in}}$ = (1.0, 0, 0) m/s and T_{in} = 300.35 K. The convergence criterion for the inverse identification was again $|O_{new} - O_{old}| < 0.001$.

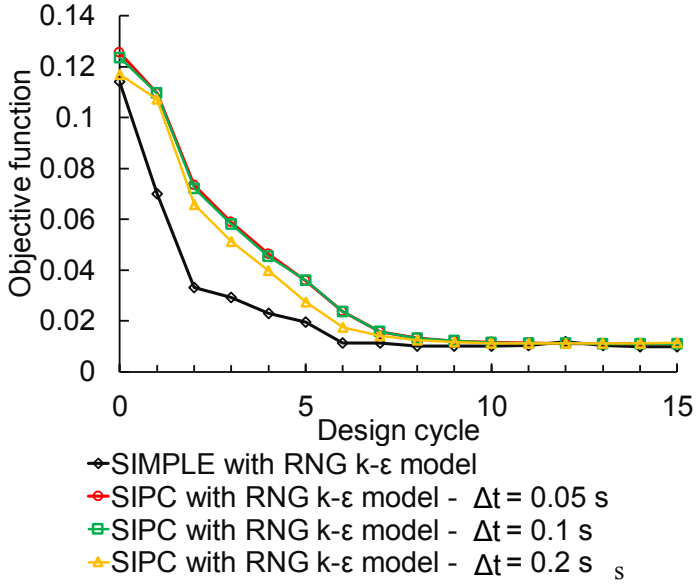

Figure 18. Objective function versus design cycle

Figure 18 shows the objective function versus the design cycle. All the designs converged and led the objective to very small values. The convergence speed differed slightly between the FFD-based adjoint method and CFD-based adjoint method because of the difference in predicted flow fields and adjoint fields. However, the convergence trajectories for the FFD-based adjoint method were almost the same for different time step sizes. This is because the Navier-Stokes/adjoint equations were solved with a sufficiently long physical flow time in each design cycle. The FFD-based adjoint method with $\Delta t = 0.05$ s was again four times faster than the CFD-based adjoint method. In proportion, the FFD-based adjoint method with $\Delta t = 0.2$ s was almost 16 times faster than the CFD-based adjoint method.

Table 2. Objective function and design variables at the optimal conditions

	Objective function	$\mathbf{U}_{in}$ (m/s)	T_{in} (K)
SIMPLE algorithm	0.0096	(1.26, 0.08, 0)	296.23
SIPC with $\Delta t = 0.05$ s	0.0111	(1.30, 0,13, 0)	296.21
SIPC with $\Delta t = 0.1$ s	0.0111	(1.30, 0.13, 0)	296.20
SIPC with $\Delta t = 0.2$ s	0.0112	(1.30, 0.12, 0)	296.22

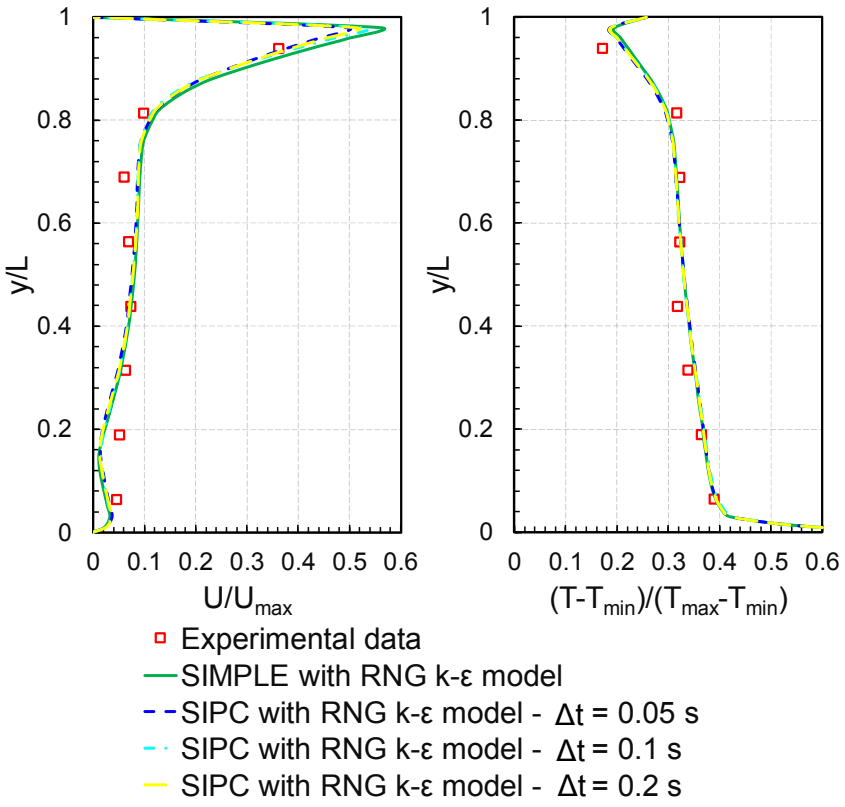

Figure 19. Comparison of the predicted air velocity and temperature profiles on the design domain with the experimental data

Table 2 summarizes the objective function and design variables at the optimal conditions. With the inversely identified optimal air supply conditions, this study conducted forward CFD simulations. We then compared the predicted air velocity and temperature profiles on the design domain with the experimental data, as shown in Figure 19. The predicted air velocity and temperature profiles were similar and agreed well with the experimental data, which confirmed the inverse identification.

4.3.3 Inverse design of the thermal environment in an aircraft cabin

Finally, this investigation conducted an inverse design of the thermal environment in a single-aisle, fully occupied aircraft cabin in order to find the optimal air supply locations, size, and parameters for the diffusers. To decrease the computing load, this study performed calculations for only half of one row of the cabin, as illustrated in Figure 20. For all the boundary conditions that did not vary in the design, one can refer to Liu et al. (2015b). This study used a modified predicted mean vote for air cabins (PMVc) developed by Cui and Zhu (2015) to evaluate the thermal comfort level. The thermal resistance of the passengers' clothing was assumed to be 0.57 clo for summer (ASHRAE, 2007). The design domain Ω was set as the area 0.1 m away from the passengers. The objective function could then be constructed as:

$$O(\xi) = \int_{\Omega} (PMV_c)^2 d\Omega \Big/ \int_{\Omega} d\Omega \tag{35}$$

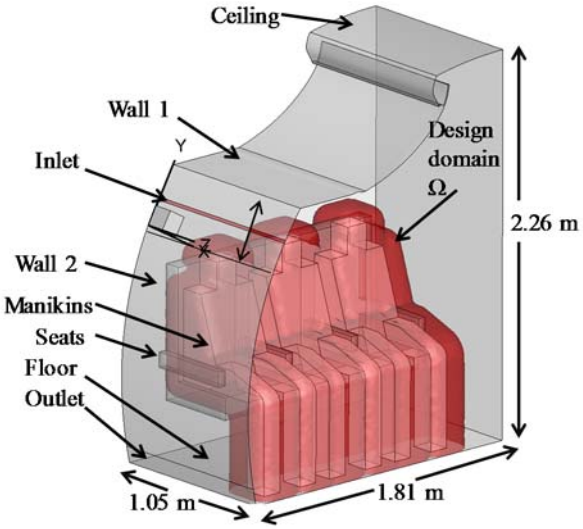

Figure 20. Schematic of the computational domain and design domain for the aircraft cabin

The FFD-based adjoint method used the SIPC scheme with a time step size of 0.1 s. The SIPC scheme solved the transient Navier-Stokes/adjoint equations for 100 s in each time step. The CFD-based adjoint method with the SIMPLE algorithm solved the steady-state Navier-Stokes/adjoint equations for 5,000 iterations in each design cycle to ensure convergence. The RNG k-ε model was adopted to simulate the turbulence. The initialized air supply velocity and temperature were U_{in} = (1.5, 0, 0) m/s and T_{in} = 16.1°C, respectively. To avoid longitudinal flow,

this study fixed U_z as 0 at the inlet. The convergence criterion for the inverse identification was $|O_{new} - O_{old}| < 0.01$.

Figure 21 shows the changes in objective function and air supply temperature with the design cycle. The two inverse designs both led the objective function to very small values, although the convergence speed differed slightly. The air supply temperature, which was more sensitive to the objective function, varied in the same direction in both designs. Furthermore, the optimal air supply temperatures were almost identical. This result implies that the FFD-based adjoint method is applicable to the inverse design of a complex indoor environment. The computing speed of the FFD-based adjoint method in this case was seven times faster than the CFD-based adjoint method.

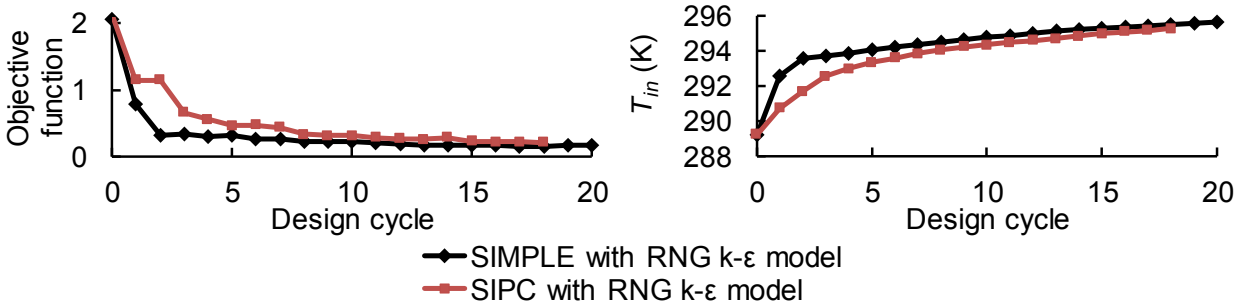

Figure 21. Changes in the objective function and air supply temperature with the design cycle

5 Discussion

To solve the adjoint equations by FFD, this study did not conduct systematic validations as we did for solving the Navier-Stokes equations. There were two reasons for this. First, because the adjoint equations are partial differential equations produced mathematically, there were no analytical solutions or experimental data for use in validation. Second, it was difficult to obtain converged numerical solutions for the adjoint equations. Applying the SIMPLE algorithm required very small relaxation factors. Since we did not know the exact solutions for the adjoint equations, this study only compared the solutions by the SIMPLE algorithm and FFD models in a simple inverse identification case, which should be sufficient in the current stage.

This study found that FFD simulations were 20 times faster than CFD simulations in predicting the transient indoor airflow. Therefore, the FFD models could be extended to the fast simulation of gaseous and particulate contaminant transport in indoor or outdoor environments (Chen and Zhao, 2011). For predicting steady-state indoor airflow, the acceleration, which depends on the time step size in FFD and the number of iterations in the SIMPLE algorithm, would not be so significant. However, in the steady-state airflow prediction by the SIMPLE algorithm, it was difficult to obtain a converged solution in the two complex indoor environments, an office with displacement ventilation and an aircraft cabin, unless small relaxation factors were used. It was then necessary to increase the number of iterations because of the reduced convergence speed. For the FFD simulations, there was no need to add relaxation in solving the Navier-Stokes

equations, and the solutions were found to be convergent. Therefore, the FFD models are also recommended for solving the steady-state indoor airflow.

6 Conclusions

This study implemented four FFD models in OpenFOAM and validated them for predicting the steady-state and transient flow in indoor environments. This study then used the FFD models to solve the adjoint equations and validated the FFD-based adjoint method for inverse identification problems and inverse designs in indoor environments. Our results led to the following conclusions:

- The NIPC-SL scheme with a turbulence model made the flow too diffusive and had the worst performance.
- The NIPC, SIPC, and RIPC schemes behaved in a similar manner and performed well in predicting both the steady-state and transient flow in indoor environment. When the same turbulence model was used, the prediction accuracy was almost the same as that with the SIMPLE algorithm. The FFD models were more than 20 times faster than the SIMPLE algorithm in predicting the transient flow.
- A larger time step size affected the accuracy of transient FFD predictions at the beginning of the simulation. For the steady-state flow predictions, the effect of time step size was minimal.
- The FFD models performed well in solving the adjoint equations. The FFD-based adjoint method was able to identify the optimal air supply conditions in the indoor environment. The FFD-based adjoint method was 4-16 times faster than the CFD-based adjoint method in each design cycle.

Acknowledgement

This research is partially supported by the U.S. Department of Homeland Security, Science and Technology Directorate, Office of University Programs, under Grant Award 2013-ST-061-ED0001, and by the National Natural Science Foundation of China, under Grant Award 51478302. The views and conclusions contained in this document are those of the authors and should not be interpreted as necessarily representing the official policies, either expressed or implied, of the U.S. Department of Homeland Security.

References

ASHRAE, 2007. Standard 161-2007, Air quality within commercial aircraft. ASHRAE, Inc., Atlanta, GA.

Blay, D., Mergui, S. and Niculae, C., 1992. Confined turbulent mixed convection in the presence of a horizontal buoyant wall jet. Fundamentals of Mixed Convection, 213, pp.65–72.

Bryson, A.E., 1975. Applied optimal control: Optimization, estimation and control. CRC Press.

Chen, C. and Zhao, B., 2011. Review of relationship between indoor and outdoor particles: I/O ratio, infiltration factor and penetration factor. Atmospheric Environment, 45(2), pp.275-288.
Chen, Q. and Xu, W., 1998. A zero-equation turbulence model for indoor airflow simulation. Energy and Buildings, 28(2), pp.137-144.
Chorin, A.J., 1967. A numerical method for solving incompressible viscous flow problems. Journal of Computational Physics, 2(1), pp.12-26.
Chorin, A.J., 1968. Numerical solution of the Navier-Stokes equations. Mathematics of Computation, 22(104), pp.745-762.
Cui, W. and Zhu, Y., 2015. Systematic study on passengers' thermal comfort under low-air-pressure environment in commercial aircraft cabin. Annual Meeting of the Center for Cabin Air Reformative Environment, Chongqing, China.
Ferziger, J.H. and Peric, M., 2012. Computational methods for fluid dynamics. Springer Science & Business Media.
Goda, K., 1979. A multistep technique with implicit difference schemes for calculating two- or three-dimensional cavity flows. Journal of Computational Physics, 30(1), pp.76-95.
Guermond, J.L., Minev, P. and Shen, J., 2005. Error analysis of pressure-correction schemes for the time-dependent Stokes equations with open boundary conditions. SIAM Journal on Numerical Analysis, 43(1), pp.239-258.
Jameson, A., 1995. Optimum aerodynamic design using CFD and control theory. AIAA paper, 1729, pp.124-131.
Jin, M., Zuo, W. and Chen, Q., 2012. Improvements of fast fluid dynamics for simulating air flow in buildings. Numerical Heat Transfer, Part B: Fundamentals, 62(6), pp.419-438.
Li, K., Su, H., Chu, J. and Xu, C., 2013. A fast-POD model for simulation and control of indoor thermal environment of buildings. Building and Environment, 60, pp.150-157.
Lin, C.H., Dunn, K.H., Horstman, R.H., Topmiller, J.L., Ahlers, M.F., Bennett, J.S., Sedgwick, L.M. and Wirogo, S., 2005. Numerical simulation of airflow and airborne pathogen transport in aircraft cabins--Part I: Numerical simulation of the flow field. ASHRAE Transactions, 111(1).
Liu, W. and Chen, Q., 2015. Optimal air distribution design in enclosed spaces using an adjoint method. Inverse Problems in Science and Engineering, 23(5), pp.760-779.
Liu, W., Duan, R., Chen, C., Lin, C.H. and Chen, Q., 2015b. Inverse design of the thermal environment in an airliner cabin by use of the CFD-based adjoint method. Energy and Buildings, 104, pp.147-155.
Liu, W., Jin, M., Chen, C., You, R. and Chen, Q., 2016b. Implementation of a fast fluid dynamics model in OpenFOAM for simulating indoor airflow. Numerical Heat Transfer, Part A: Applications, 69(7), pp.748-762.
Liu, W., You, R., Xue, Y., and Chen, Q., 2016a. Comparison and integration of CFD-based genetic algorithm and adjoint method for the inverse design of indoor environment. Proceedings of the 14th International Conference on Indoor Air Quality and Climate (Indoor Air 2016), Paper 347, 8 pages, Ghent, Belgium.
Liu, W., Zhang, T., Xue, Y., Zhai, Z.J., Wang, J., Wei, Y., and Chen, Q., 2015a. State-of-the-art methods for inverse design of an enclosed environment. Building and Environment, 91, pp.91-100.
Miller, B.L. and Goldberg, D.E., 1995. Genetic algorithms, tournament selection, and the effects of noise. Complex Systems, 9(3), pp.193-212.

OpenFOAM, 2007. The Open Source CFD Toolbox, http://www.opencfd.co.uk/openfoam.html.
Othmer, C., de Villiers, E. and Weller, H.G., 2007. Implementation of a continuous adjoint for topology optimization of ducted flows. In 18th AIAA Computational Fluid Dynamics Conference, June.
Patankar, S.V. and Spalding, D.B., 1972. A calculation procedure for heat, mass and momentum transfer in three-dimensional parabolic flows. International Journal of Heat and Mass Transfer, 15(10), pp.1787-1806.
Stam, J., 1999. Stable fluids. In Proceedings of the 26th annual conference on computer graphics and interactive techniques (pp. 121-128). ACM Press/Addison-Wesley Publishing Co.
Staniforth, A. and Côté, J., 1991. Semi-Lagrangian integration schemes for atmospheric models-A review. Monthly Weather Review, 119(9), pp.2206-2223.
Temam, R., 1969. Sur l'approximation de la solution des équations de Navier-Stokes par la méthode des pas fractionnaires (II). Archive for Rational Mechanics and Analysis, 33(5), pp.377-385.
Timmermans, L.J.P., Minev, P.D. and Van De Vosse, F.N., 1996. An approximate projection scheme for incompressible flow using spectral elements. International Journal for Numerical Methods in Fluids, 22(7), pp.673-688.
Wang, M. and Chen, Q., 2009. Assessment of various turbulence models for transitional flows in an enclosed environment (RP-1271). HVAC&R Research, 15(6), pp.1099-1119.
Xue, Y., Liu, W. and Zhai, Z.J., 2016. New semi-Lagrangian-based PISO method for fast and accurate indoor environment modeling. Building and Environment, 105, pp.236-244.
Xue, Y., Zhai, Z. J., and Chen, Q., 2013. Inverse prediction and optimization of flow control conditions for confined spaces using a CFD-based genetic algorithm. Building and Environment, 64, pp.77-84.
Yakhot, V.S., Orszag, S.A., Thangam, S., Gatski, T.B., and Speziale, C.G., 1993. Development of turbulence models for shear flows by a double expansion technique. Physics of Fluids A: Fluid Dynamics, 4(7), pp.1510-1520.
Yuan, X., Chen, Q., Glicksman, L.R., Hu, Y. and Yang, X., 1999. Measurements and computations of room airflow with displacement ventilation. ASHRAE Transactions, 105, p.340.
Zhang, Z., Zhang, W., Zhai, Z.J. and Chen, Q.Y., 2007. Evaluation of various turbulence models in predicting airflow and turbulence in enclosed environments by CFD: Part 2—Comparison with experimental data from literature. HVAC&R Research, 13(6), pp.871-886.
Zuo, W. and Chen, Q., 2009. Real-time or faster-than-real-time simulation of airflow in buildings. Indoor Air, 19(1), pp.33-44.
Zuo, W., Hu, J. and Chen, Q., 2010. Improvements in FFD modeling by using different numerical schemes. Numerical Heat Transfer, Part B: Fundamentals, 58(1), pp.1-16.